

FULL ARTICLE

# Chemically-specific dual/differential CARS micro-spectroscopy of saturated and unsaturated lipid droplets

Claudia Di Napoli<sup>1</sup>, Francesco Masia<sup>2</sup>, Iestyn Pope<sup>1</sup>, Cees Otto<sup>3</sup>, Wolfgang Langbein<sup>2</sup>, and Paola Borri<sup>\*1,2</sup>

<sup>1</sup> Cardiff University School of Biosciences, Museum Avenue, Cardiff CF10 3AX, United Kingdom

<sup>2</sup> Cardiff University School of Physics and Astronomy, The Parade, Cardiff CF24 3AA, United Kingdom

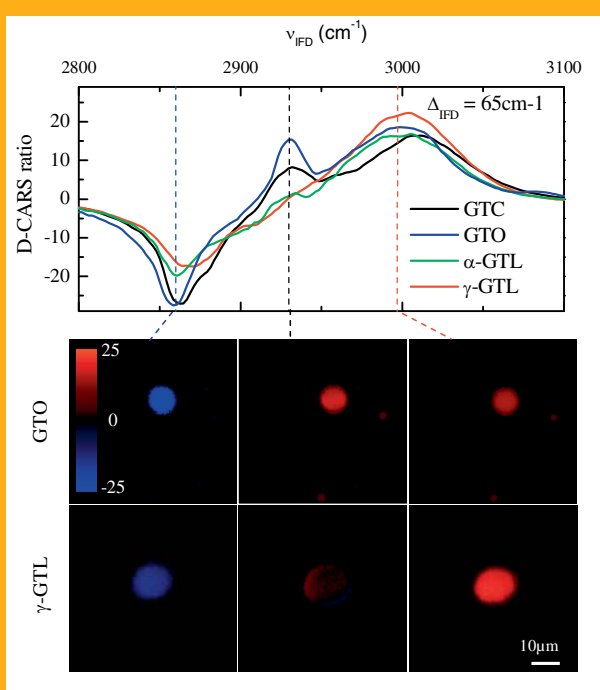
<sup>3</sup> University of Twente, Faculty of Science and Technology, Drienerlolaan 5, 7500 AE Enschede, The Netherlands

Received 1 October 2012, revised 4 November 2012, accepted 6 November 2012

Published online 30 November 2012

**Key words:** Multiphoton microscopy, nonlinear optics, Coherent Antistokes Raman Scattering, lipids

We have investigated the ability of dual-frequency Coherent Antistokes Raman Scattering (D-CARS) micro-spectroscopy, based on femtosecond pulses (100 fs or 5 fs) spectrally focussed by glass dispersion, to distinguish the chemical composition of micron-sized lipid droplets consisting of different triglycerides types (polyunsaturated glyceryl trilinolenate, mono-unsaturated glyceryl trioleate and saturated glyceryl tricaprlylate and glyceryl tristearate) in a rapid and label-free way. A systematic comparison of Raman spectra with CARS and D-CARS spectra was used to identify D-CARS spectral signatures which distinguish the disordered poly-unsaturated lipids from the more ordered saturated ones both in the CH-stretch vibration region and in the fingerprint region, without the need for lengthy CARS multiplex acquisition and analysis. D-CARS images of the lipid droplets at few selected wavenumbers clearly resolved the lipid composition differences, and exemplify the potential of this technique for label-free chemically selective rapid imaging of cytosolic lipid droplets in living cells.



Measured D-CARS spectra in the CH-Strech region for lipid droplets (LDs) of different lipid composition as indicated. The bottom panels show images through the equatorial plane of LDs at wavenumbers indicated by the corresponding dashed lines.

\* Corresponding author: e-mail: borrip@cardiff.ac.uk, Phone: +44 29 20879356

This is an open access article under the terms of the Creative Commons Attribution License, which permits use, distribution and reproduction in any medium, provided the original work is properly cited.

## 1. Introduction

Historically considered as inert fat particles, cytosolic lipid droplets (LDs) have been outside the focus of research until recently, but are now being recognized as dynamic organelles with complex and interesting biological functions, beyond mere energy storage, relevant for lipid homeostasis and the pathophysiology of metabolic diseases [1, 2]. LDs are found in most cell types, including plants, and consist of a hydrophobic core containing neutral lipids, mainly triglycerides and sterol esters, surrounded by a phospholipid monolayer. Among the several unanswered questions regarding LDs is their heterogeneity in size and composition and how this is regulated in cells. LDs show a large range of sizes from 0.1  $\mu\text{m}$  to 100  $\mu\text{m}$ , depending on the cell type, and there is increasing evidence that their lipid composition (e.g. saturated versus unsaturated acyl chains) varies between different droplets and even within a single droplet. Understanding the role of lipid composition in LDs could have implications in e.g. discovering the cellular mechanisms by which the quality of dietary fat influences our health.

Imaging LDs in cells using fluorescence staining of lipids is known to be prone to labeling artifacts, be unspecific, often require cell fixation [3], and suffer from photo-bleaching. A more specific technique to distinguish lipid composition uses electron dense osmium tetroxide which preferentially binds unsaturated fatty acid chains and is visible with electron microscopy, a method however limited by laborious sample preparation and not suitable for imaging living cells [4]. Coherent Antistokes Raman Scattering (CARS) microscopy has emerged in the last decade as a powerful multiphoton microscopy technique to image LDs label-free and with intrinsic three-dimensional spatial resolution in living cells [5–7]. In CARS two laser fields, pump and Stokes of frequencies  $\nu_P$  and  $\nu_S$  respectively, are used to coherently drive intrinsic molecular vibrations via their interference at the frequency difference  $\nu_P - \nu_S$ . In the two-pulse version, the pump field itself is used to probe the vibrations via the Anti-Stokes Raman scattering at  $2\nu_P - \nu_S$ . Compared to spontaneous Raman, CARS benefits from the constructive interference of the Raman scattered light of many identical bonds coherently driven in the focal volume. Therefore, the technique has proven to be especially advantageous to image cytosolic LDs of size  $\gtrsim 0.5 \mu\text{m}$  in diameter (comparable or larger than the focal volume of a high numerical aperture objective) through the numerous CH bonds in the acyl chain of fatty acids.

To gain the degree of chemical specificity required to distinguish lipids of different chemical composition in CARS microscopy it is however not sufficient to resonantly drive a single frequency. For

this purpose multiplex CARS micro-spectroscopy was implemented, where several vibrational frequencies are simultaneously excited and probed and a CARS spectrum carrying detailed information of the different vibrational components is recorded for every spatial point in the image. With this method, it was possible to image and quantitatively analyze the heterogeneous lipid composition of LDs in mouse adipocytes (3T3-L1 cells) [8]. The advantage of multiplex-CARS is that complex CARS spectra acquired over a sufficiently wide range can be quantitatively interpreted using fitting procedures (e.g. the maximum entropy method [9]) that allow reconstruction of the corresponding spontaneous Raman scattering spectra. The disadvantage of the method is however its low image speed, since the acquisition time for a single CARS spectrum is typically in the 10 ms range resulting in tens of minutes for the acquisition of spatially-resolved 3D images. Consequently, the work in Ref. [8] was performed on fixed cells, defeating the purpose of CARS microscopy as a live cell imaging technique.

We recently demonstrated a new method to perform dual-frequency/differential CARS (D-CARS) employing linearly chirped femtosecond laser pulses which simultaneously excite and probe two vibrational frequencies adjustable in center and separation. The resulting sum and difference CARS intensities are detected by a fast and efficient single photomultiplier (PMT), thus maintaining the high image speed of single-frequency CARS microscopy and offering at the same time improved chemical specificity and image contrast against the non-resonant CARS background [10, 11]. In the present work, we have applied this D-CARS method to a series of LD model systems (micron-sized LDs in agarose gel consisting of unsaturated, mono-saturated or poly-saturated triglycerides) and demonstrate its ability to distinguish between the different lipid types while maintaining rapid imaging speed. These results exemplify the potential of our D-CARS method for label-free chemically selective rapid imaging of cytosolic LDs in living cells.

## 2. Experimental

### 2.1 Spontaneous Raman spectroscopy set-up

Spontaneous Raman spectra were taken using two confocal micro-spectroscopy set-ups. Specifically, confocal Raman spectra of glyceryl tricaprilate and glyceryl tristearate LDs were taken using a Ti-U microscope stand with a  $20 \times 0.75$  NA objective. The 532 nm laser excitation was filtered with a Semrock LL01-532 and coupled into the microscope by a di-

chroic mirror (Semrock LPD01-532RS), with a power of 10 mW at the sample. The Raman scattering was collected in epi-direction, filtered with a long pass filter (Semrock BLP01-532R), dispersed by an imaging spectrometer (Horiba iHR550) with a 600 lines/mm grating and detected with a CCD Camera (Andor Newton DU971N-BV) with a FWHM spectral resolution of  $2.3 \text{ cm}^{-1}$ . Raman spectra for the other lipids in this work were taken using the set-up described in details in Ref. [12] with a laser excitation at 647 nm, a  $40 \times 0.95 \text{ NA}$  objective, a power of 35 mW onto the sample and a high-resolution spectrograph providing  $2.25 \text{ cm}^{-1}$  spectral resolution. All measurements were performed at room temperature.

## 2.2 CARS micro-spectroscopy set-up

For D-CARS micro-spectroscopy two set-ups were used. The first set-up is based on a 100 fs laser system and is described in Ref. [10, 13]. Briefly, a Ti:Sapphire laser source (Coherent Mira) delivering 100 fs Stokes pulses centered at 832.5 nm with  $1/T = 76 \text{ MHz}$  repetition rate synchronously pumps an optical parametric oscillator (APE PP2) which is intracavity frequency doubled providing 100 fs pump pulses centered at 670 nm. Pump and Stokes pulses travel through a glass (SF57) block of 9 cm length, and the Stokes travels through an additional 8 cm of SF57. The chirp introduced by the remaining optics including the microscope objective was equivalent to 4 cm SF57. In this way, the linear chirp of pump and Stokes was adjusted to be similar to achieve spectral focussing and corresponded to an excitation spectral resolution of  $30 \text{ cm}^{-1}$  and a chirped pump pulse duration of 700 fs. This degree of linear chirp is a compromise between CARS spectral selectivity and signal strength [13]. The delay time  $t_0$  between pump and Stokes controls their instantaneous frequency difference  $\nu_{\text{IFD}}$ , enabling to measure CARS intensity spectra  $I_{\text{CARS}}(\nu_{\text{IFD}}(t_0))$  by simply moving a delay line. To measure D-CARS, the pump-Stokes pair is divided into two orthogonally polarized pairs ( $\Pi_1$ ,  $\Pi_2$ ) with adjustable relative powers.  $\Pi_2$  travels through an additional  $d = 4 \text{ mm}$  thin SF57 glass element and is delayed by  $T/2$  before being recombined with  $\Pi_1$ . This creates a periodic pulse sequence with  $\Pi_1$  driving a vibrational resonance  $\nu_{\text{IFD1}}$  tuneable via  $t_0$  and  $\Pi_2$  driving a shifted resonance  $\nu_{\text{IFD2}}$  with the frequency difference  $\Delta_{\text{IFD}} = \nu_{\text{IFD1}} - \nu_{\text{IFD2}} = 65 \text{ cm}^{-1}$  being determined by the additional thickness  $d$ . A home built microscope comprised a 1.2 numerical aperture (NA) water immersion objective (Leica HCX PL APO  $63 \times \text{W Corr CS}$ ) to focus the exciting beams and an identical objective to collect the CARS in transmission

direction. The set-up provided  $xy$  beam and  $xyz$  sample scanning, where  $x$ ,  $y$  are the transversal directions and  $z$  is the axial direction of the focussed beam. The CARS intensity generated by each pair is detected simultaneously using a single PMT and appropriate high-pass/low-pass frequency filtering of the PMT current and high-frequency detection electronics at the laser repetition rate (see Ref. [10]).

The second set-up is based on a single ultrafast laser source, similar to Ref. [11], except here we used a Ti:Sapphire laser (Venteon Pulse:One PE) delivering 5 fs pulses with a spectrum covering the range 660 nm to 970 nm above 10% peak intensity and a repetition rate of 80 MHz. By an appropriate sequence of dichroic beam splitters, the laser spectrum is split into a pump and a Stokes part centered at 682 nm and 806 nm with a bandwidth of 65 nm and 200 nm, respectively. The remaining infrared portion of the laser spectrum (930–970 nm) can be compressed to 30 fs pulses at the sample and used for two-photon fluorescence excitation and second harmonic generation simultaneously with CARS, but this option was not utilized here and will be discussed in a forthcoming work [14]. Pump and Stokes were linearly chirped using SF57 glass blocks similar to what discussed above, and enabled CARS spectroscopy by varying the delay time  $t_0$  between pump and Stokes over the vibrational range of 1200–3500  $\text{cm}^{-1}$ , with a spectral resolution of about  $30 \text{ cm}^{-1}$  in the 1200–2200  $\text{cm}^{-1}$  range and about  $15 \text{ cm}^{-1}$  in the 2200–3500  $\text{cm}^{-1}$  range. The former was limited by a non-perfect spectral focussing over the entire tuning range due to third-order glass dispersion (an effect which can be compensated by changing the SF57 glass length for the different spectral regions). D-CARS was performed as discussed above for the setup with 100 fs pulses, and two IFD differences were considered, namely  $\Delta_{\text{IFD}} = 68 \text{ cm}^{-1}$  and  $\Delta_{\text{IFD}} = 20 \text{ cm}^{-1}$ . Pump and Stokes pulses were coupled into a commercial inverted microscope stand (Nikon Ti-U) via a home-built beam-scanning head. The microscope was equipped with a  $20 \times 0.75 \text{ NA}$  dry objective (Nikon CFI Plan Apo  $\lambda$ ) to focus the beams onto the sample and a  $0.72 \text{ NA}$  dry condenser for CARS collection in transmission direction. A motorized sample stage enabled  $xy$  sample movement and a motorized objective focussing enabled  $z$  movement. CARS was spectrally discriminated by appropriate band pass filters and detected by a PMT (Hamamatsu H7422-40). Noticeably this set-up is specifically designed for biological applications. CARS and D-CARS alignments are mostly hands-off via remote computer-controlled optics adjustments hence user-friendly. More details on the setup will be published in a forthcoming work [14]. All measurements were performed at room temperature.

### 2.3 Lipid droplet samples

Lipids were purchased from Sigma-Aldrich® (Zwijndrecht, the Netherlands) and from Nu-Chek Prep, Inc (Elysian, Minnesota, USA). The following five triglycerides were investigated: glyceryl tricaprilate (GTC) with C8:0 fatty acid saturated chains; glyceryl tristearate (GTS) with C18:0 fatty acid saturated chains; glyceryl trioleate (GTO) with C18:1 mono-unsaturated chains with *cis* double bond at the 9th position from the first carbon atom in the chain (*1,2,3-Tri(cis-9-octadecenoyl)glycerol*);  $\alpha$ -glyceryl trilinolenate ( $\alpha$ -GTL) with C18:3 fatty acid chains and all *cis* double bonds at 9, 12, and 15th position from the 1st carbon atom (*1,2,3-Tri-(cis,cis,cis-9,12,15-octadecatrienoyl)glycerol*);  $\gamma$ -glyceryl trilinolenate ( $\gamma$ -GTL) with C18:3 fatty acid chains all *cis* double bonds at the 6th, 9th and 12th position from the 1st carbon atom (*1,2,3-Tri-(cis,cis,cis-6,9,12-octadecatrienoyl)glycerol*).

At room temperature GTS is in solid phase, while the other lipids in liquid phase (melting temperatures are 9–10 °C for GTC, –5.5 °C for GTO, –24 °C for  $\alpha$ -GTL, and 71–73 °C for GTS).

The samples consist of micron-sized lipid droplets suspended in a solution of 2% low melting temperature (65 °C) agarose powder and 98% water. Droplets were created by adding a given lipid type in the agar-water solution with a 1% volume-volume ratio and by sonicating the obtained emulsion for 15 minutes at 80 °C. 13  $\mu$ L are pipetted inside a 120  $\mu$ m thick imaging spacer (Grace™Bio-Lab SecureSeal™) glued on a glass coverslip in order to create a chamber, which is sealed afterwards by a second coverslip. Samples were stored in 100% humidity conditions in order to prevent drying of the agar emulsion.

### 3. Results and discussion

To characterize the Raman spectral features of the different lipid types investigated here and for comparison with CARS intensity spectra  $I_{\text{CARS}}(\nu_{\text{IFD}})$ , spontaneous Raman spectra were measured for all triglycerides LD samples. Additionally, spectra of LDs made of oleic acid (OA) were measured. All spectra are shown in Figure 1, normalized to the area in the CH-stretch region (2750–3050  $\text{cm}^{-1}$ ) which provides a good measure of the total lipid concentration [8]. Several bands are observed, with two spectral regions being characteristic for lipids with different molecular structures, namely the fingerprint (700–2000  $\text{cm}^{-1}$ ) and the CH-stretch regions. As discussed in literature [15, 16], the fingerprint region is characterized by a band between

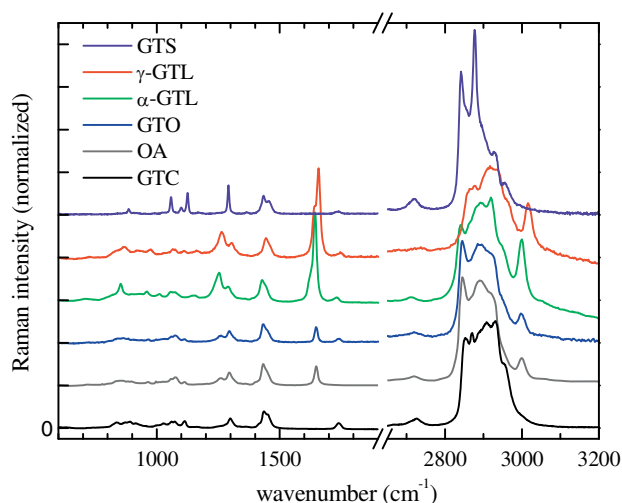


**Figure 1** Raman spectra at room temperature of micron-sized lipid droplets in agarose gel made from different lipids as indicated. GTC: glyceryl tricaprilate. GTO: glyceryl trioleate. OA: oleic acid.  $\alpha(\gamma)$ -GTL:  $\alpha(\gamma)$ -glyceryl trilinolenate, GTS: glyceryl tristearate. Curves are vertically shifted for clarity.

1050  $\text{cm}^{-1}$  and 1150  $\text{cm}^{-1}$  due to the C–C stretch, a band around 1290  $\text{cm}^{-1}$  due to CH<sub>2</sub> twist, and the band between 1400  $\text{cm}^{-1}$  and 1500  $\text{cm}^{-1}$  due to CH<sub>2</sub> and CH<sub>3</sub> deformations. In the unsaturated lipids (OA, GTO and GTL) the band around 1290  $\text{cm}^{-1}$  broadens and splits into two bands around 1260  $\text{cm}^{-1}$  and 1300  $\text{cm}^{-1}$  attributed to =CH and CH<sub>2</sub> deformations respectively, with the relative intensity of the former increasing with increasing numbers of double bonds. A similar trend occurs for the band around 1660  $\text{cm}^{-1}$  attributed to the C=C stretch, which is absent in saturated lipids (GTC and GTS), appears for GTO and OA and strengthens for GTL. The weak band around 1740  $\text{cm}^{-1}$  is attributed to the C=O stretch from the ester bonds between glycerol and the fatty acids, and is indeed absent in the OA.

The CH stretch region is congested with several overlapping resonances complicating the attribution. The 2850  $\text{cm}^{-1}$  band is due to the CH<sub>2</sub> symmetric stretch, shifting towards lower wavenumbers for saturated lipids in the solid phase (see spectrum of GTS). The 2880  $\text{cm}^{-1}$  band is due to the CH<sub>2</sub> asymmetric stretch enhanced by the Fermi resonance interaction with the overtones of CH<sub>2</sub> and CH<sub>3</sub> deformations, especially prominent for lipids in the solid phase, such that the intensity ratio between the 2880  $\text{cm}^{-1}$  and 2850  $\text{cm}^{-1}$  bands can be used as a measure of the acyl chain order [8]. The 2930  $\text{cm}^{-1}$  band is a combination of CH<sub>3</sub> stretch vibrations and CH<sub>2</sub> asymmetric stretch enhanced by the broadening and shift of the CH deformations in the liquid phase,

hence its intensity relative to the  $2850\text{ cm}^{-1}$  band can be used as a measure of disorder. The  $=\text{CH}$  stretch gives rise to a band around  $3010\text{ cm}^{-1}$ , with an intensity proportional to the number of carbon-carbon double bonds present in the main lipid chain, which is highest for GTL. GTS is solid at room temperature and exhibits the prominent  $2880\text{ cm}^{-1}$  band while the other lipids which are liquid at room temperatures exhibit a significant band around [16]  $2930\text{ cm}^{-1}$ . The band around  $2730\text{ cm}^{-1}$  is likely [17, 18] due to a combination overtone of  $\text{CH}_2$  scissor and wag, enhanced by the proximity of the Fermi resonance with the  $\text{CH}_2$  stretch.

### 3.1 Single-pair CARS

It is well known that CARS intensity spectra do not resemble Raman spectra due to the interference between the resonant and non-resonant terms in the third-order susceptibility describing the CARS field [9]. For the application of D-CARS, our aim is to determine whether the *difference* between CARS intensities at suitable frequencies does provide a reliable information on the specific lipid type and can be directly used for rapid chemically-specific imaging, hence overcoming the drawback of slow acquisition speeds of multiplex CARS microscopy. For this purpose, we first measured the CARS intensity spectra  $I_{\text{CARS}}(\nu_{\text{IFD1}})$  of the LD samples using the pulse pair  $\Pi_1$  (see Section 2.2). Results are shown in Figure 2 using the 100 fs laser system and in Figure 3 using the 5 fs laser system. Figure 2a shows the CARS intensity  $I_{\text{CARS}}(\nu_{\text{IFD1}}(t_0))$  measured as a function of the delay time  $t_0$  between pump and Stokes pulses corresponding to  $\nu_{\text{IFD1}}$  in the  $\text{CH}$ -stretch region [13, 19] on a GTO LD of  $4\text{ }\mu\text{m}$  diameter taken at the LD center such that the focal volume was inside the LD.  $I_{\text{CARS}}(x, t_0)$  (see inset in Figure 2a) for  $y, z$  in the center of the LD was acquired to determine the CARS intensity at the LD and in the surrounding agarose gel, as indicated by the dotted lines. The Gaussian shape of the CARS intensity spectrum in the agarose gel mainly reflects the pump-Stokes intensity cross-correlation when varying temporal overlap. However, due to the tail of the water resonance at  $\sim 3200\text{ cm}^{-1}$  this profile is not exactly equal to the non-resonant CARS response from the cross-correlation of the Gaussian pulses, as shown by the same measurement taken on the glass coverslip. To represent CARS spectral “strengths” independent of excitation/detection parameters, we normalize  $I_{\text{CARS}}(\nu_{\text{IFD1}})$  to the non-resonant CARS intensity of glass  $I_{\text{CARS}}^{\text{NR}}(\nu_{\text{IFD1}})$  resulting in the CARS ratio  $\hat{I}_{\text{CARS}} = I_{\text{CARS}}/I_{\text{CARS}}^{\text{NR}}$  shown in Figure 2b, c. Corresponding Raman spectra are also shown for direct comparison in the same wavenumber range.

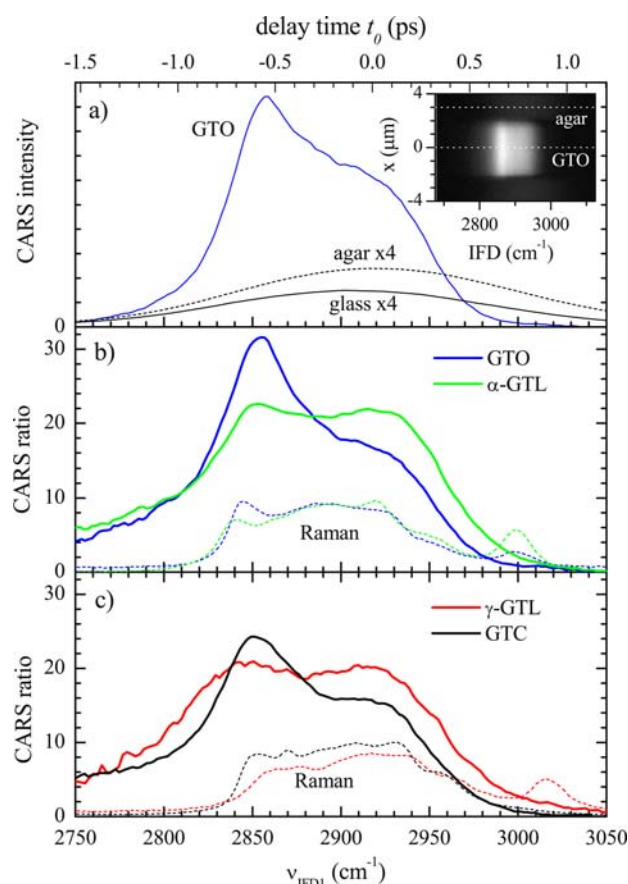


**Figure 2** CARS measured with the 100 fs laser system. (a)  $I_{\text{CARS}}$  measured on a  $4\text{ }\mu\text{m}$  LD of GTO, in the surrounding agarose gel and in the glass coverslip as a function of the delay time  $t_0$  between pump and Stokes pulses and corresponding  $\nu_{\text{IFD1}}$ . The inset shows a  $I_{\text{CARS}}(x, t_0)$  for  $(y, z)$  at the center of the LD, with dotted lines indicating the  $x$  positions of GTO and agar. Pump power on the sample 7 mW, Stokes power 2 mW, objective  $60\times 1.2\text{ NA}$ , 0.1 ms pixel dwell time, 75 nm pixel size. (b) and (c) CARS ratio  $\hat{I}_{\text{CARS}}$  in LDs of different lipids as indicated. Raman spectra (dotted lines) are also shown for comparison.

Due to the interference between the resonant and non-resonant terms in the third-order susceptibility, low wavenumber edges are enhanced and high wavenumber edges are suppressed in CARS compared to spontaneous Raman, as seen here for the enhanced  $\text{CH}_2$  symmetric stretch at  $2850\text{ cm}^{-1}$ . Nevertheless, the relative intensity of the band at  $2930\text{ cm}^{-1}$  with respect to the band at  $2850\text{ cm}^{-1}$  follows the same trend as in spontaneous Raman, being higher for the more disordered poly-unsaturated GTL compared to the saturated and mono-unsaturated lipids. Similar results were obtained by measuring the CARS spectra in the  $\text{CH}$ -stretch region with the 5 fs laser system (see Figure 3 right panels), which enabled to address a broader spec-

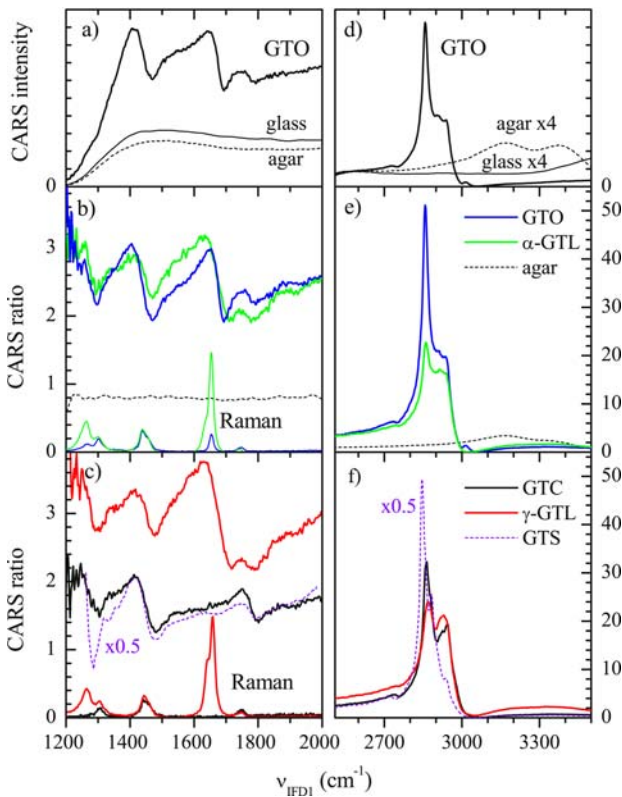


**Figure 3** CARS measured with the 5 fs laser system in the fingerprint region (a–c) and in the CH-stretch region (d–f). (a) and (d)  $I_{\text{CARS}}$  measured on a  $> 2 \mu\text{m}$  lipid droplet of GTO, in the agarose gel and in the glass coverslip. (b) and (c) CARS ratio  $\hat{I}_{\text{CARS}}$  for different lipid types and agar as indicated, together with corresponding Raman spectra in the fingerprint region. (e) and (f) as (b) and (c), but for the CH-stretch region. Pump power on the sample 16 mW, Stokes power 8 mW, objective  $20 \times 0.75 \text{ NA}$ .

tral range with a better spectral resolution (see Section 2.2).

With the 5 fs laser system we could also measure CARS spectra in the fingerprint region (see Figure 3 left panels). In this region the resonant CARS contribution is smaller than the non-resonant term and the spectral lineshape is dominated by the interference term [5, 11]  $2\chi_{\text{NR}}^{(3)}\Re\{\chi_R^{(3)}\}$  between the resonant part of the third-order susceptibility  $\chi_R^{(3)} = R/(-\omega_\delta - i\Gamma)$  and the real non-resonant part  $\chi_{\text{NR}}^{(3)}$ . Here  $\omega_\delta$  is the difference between vibrational excitation and resonance frequency [19], and  $\Gamma$  is the vibrational dephasing rate. This creates a dispersive lineshape  $\Re\{\chi_R^{(3)}\} = -R\omega_\delta/(\omega_\delta^2 + \Gamma^2)$  which is spectrally extended with tails  $\propto \omega_\delta^{-1}$ . Hence single-frequency CARS is less suited to create specific vibrational contrast than spontaneous Raman, which has a lineshape proportional to  $\Im\{\chi_R^{(3)}\} = R\Gamma/(\omega_\delta^2 + \Gamma^2)$ . Nevertheless the presence of the C=C stretch band at around

$1660 \text{ cm}^{-1}$  is clearly visible in the CARS spectra of GTL and GTO and is absent in GTS and GTC as expected. GTO also exhibits a steeper slope between maximum and minimum in the dispersive spectrum, indicative of a sharper linewidth  $\Gamma$  of the  $1660 \text{ cm}^{-1}$  band compared to GTL consistent with the Raman spectra.

### 3.2 Dual-pair differential CARS

The concept of D-CARS is visualized in Figure 4 using the CARS spectrum measured in the CH-stretch region with the 100 fs laser system on GTO and  $\alpha$ -GTL droplets. The D-CARS ratio  $\hat{I}_{\text{DCARS}} = \hat{I}_{\text{CARS}}(\nu_{\text{IFD2}}) - \hat{I}_{\text{CARS}}(\nu_{\text{IFD1}})$  is calculated from the CARS ratio of  $\Pi_1$  using  $\hat{I}_{\text{CARS}}(\nu_{\text{IFD2}}) = \hat{I}_{\text{CARS}}(\nu_{\text{IFD1}} - \Delta_{\text{IFD}})$ , i.e. the second pair  $\Pi_2$  probes a vibrational resonance at a smaller frequency shifted by  $\Delta_{\text{IFD}}$  compared to the first pair  $\Pi_1$ . The resulting D-CARS ratio spectrum is shown for  $\Delta_{\text{IFD}} = 65 \text{ cm}^{-1}$  in Figure 4b, d. The differences

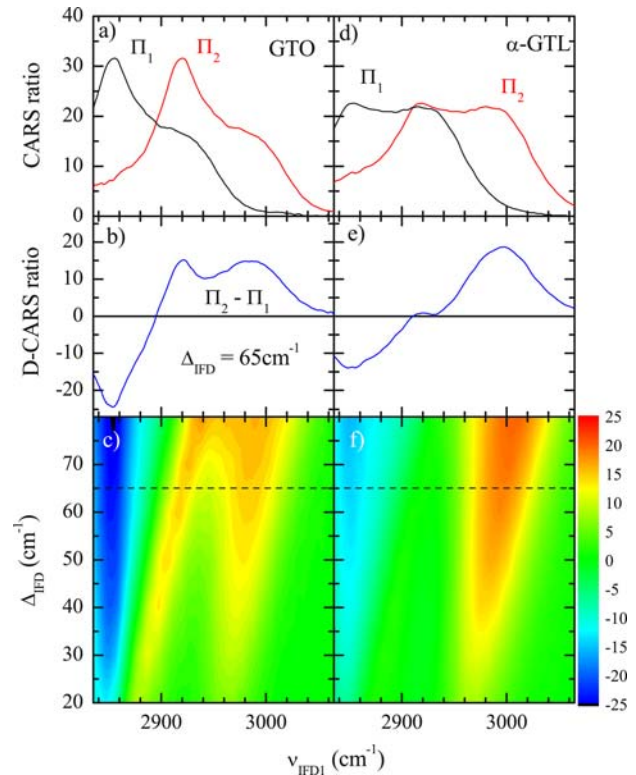


**Figure 4** CARS and D-CARS ratio versus  $\nu_{\text{IFD1}}$  calculated from the measured  $\Pi_1$  CARS for GTO (a–c) and  $\alpha$ -GTL (d–f). (a, d): CARS ratio  $\hat{I}_{\text{CARS}}$  of the two pairs  $\Pi_{1,2}$  for  $\Delta_{\text{IFD}} = 65 \text{ cm}^{-1}$ . (b, e) D-CARS ratio  $\hat{I}_{\text{DCARS}}$  for  $\Delta_{\text{IFD}} = 65 \text{ cm}^{-1}$ . (c, f) D-CARS ratio  $\hat{I}_{\text{DCARS}}$  as function of  $\Delta_{\text{IFD}}$  on a color scale as indicated.

between the single-pair CARS ratio of GTO, which has a pronounced peak at around  $2850\text{ cm}^{-1}$  and a shoulder around  $2930\text{ cm}^{-1}$ , and  $\alpha$ -GTL which has a “flat-hat” lineshape with both bands equally intense, manifest as a D-CARS ratio which is nearly zero for  $\alpha$ -GTL at  $2930\text{ cm}^{-1}$  and significantly larger than zero for GTO. Figure 4c, f show the dependence of  $\hat{I}_{\text{DCARS}}$  on  $\Delta_{\text{IFD}}$ . Considering the limited bandwidth of the 100 fs laser system, the value  $\Delta_{\text{IFD}} = 65\text{ cm}^{-1}$  chosen for the D-CARS experiment represents a compromise between having a large difference in  $\hat{I}_{\text{DCARS}}$  to distinguish GTO and GTL and maintaining sufficient temporal overlap of pump and Stokes in both pairs.

Measured D-CARS ratio spectra using both pairs are shown in Figure 5 in the CH-stretch range using both the 100 fs laser system (top panel) and the 5 fs system (center, bottom). They confirm the expected behavior from the simulations, with  $\alpha$ -GTL and  $\gamma$ -GTL exhibiting  $\hat{I}_{\text{DCARS}}(2930\text{ cm}^{-1}) \approx 0$  while GTC and GTO showing  $\hat{I}_{\text{DCARS}}(2930\text{ cm}^{-1}) > 0$ , and all the lipids have a negative D-CARS at around  $2850\text{ cm}^{-1}$  and a positive D-CARS at around  $2990\text{ cm}^{-1}$ . The bottom panels in Figure 5 show the corresponding  $\hat{I}_{\text{DCARS}}(x, y)$  images measured on the LDs, which reveal that D-CARS can be used to distinguish poly-unsaturated disordered lipids from more ordered unsaturated or mono-saturated ones by simply looking at  $\hat{I}_{\text{DCARS}}$  at a specific  $\nu_{\text{IFD}1,2}$ . Note also the suppression of the non-resonant CARS background from the agarose gel surrounding each LD in D-CARS [10].

Measured D-CARS spectra are shown in Figure 6 in the fingerprint range using the 5 fs system with a  $\Delta_{\text{IFD}} = 20\text{ cm}^{-1}$  which is comparable to the spectral resolution and the Raman linewidth of the resonances in this range. Hence  $\hat{I}_{\text{DCARS}}$  can be considered as the spectral derivative of  $\hat{I}_{\text{CARS}}$ , which for small resonant contributions is given by  $\partial_{\omega} \Re\{\chi_R^{(3)}\} = R(\omega_0^2 - \Gamma^2)/(\omega_0^2 + \Gamma^2)^2$ , and thus recover a lineshape similar to that of spontaneous Raman [11]. As expected, the C=C stretch at around  $1660\text{ cm}^{-1}$  is absent in  $\hat{I}_{\text{DCARS}}(\nu_{\text{IFD}1})$  of GTC and present for all other unsaturated lipids. The D-CARS images (bottom panels in Figure 6) measured on the LDs at the C=C stretch show the difference between the saturated GTC lipid ( $\hat{I}_{\text{DCARS}} \approx 0$ ) and the unsaturated ones ( $\hat{I}_{\text{DCARS}} > 0$ ), demonstrating that D-CARS at specific wavenumbers is a valuable tool to chemically distinguish saturated from unsaturated lipids. We note however that the values of  $\hat{I}_{\text{DCARS}}$  from resonant contributions in the fingerprint wavenumber region are much lower than in the CH-stretch, hence small alignment artifacts due to e.g. non-perfect spatial overlap of  $\Pi_1$  and  $\Pi_2$  become critical. This is for example the case in the images shown for GTL where a spatial differential is visible. We also note that although GTL has three

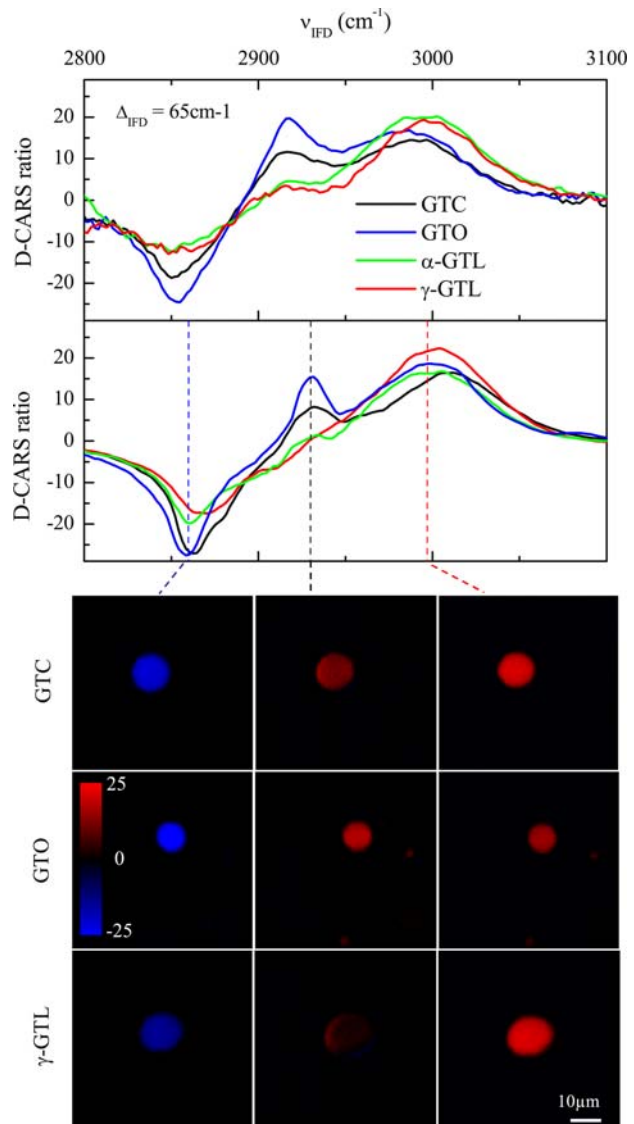


**Figure 5** Measured  $\hat{I}_{\text{DCARS}}$  spectra in the CH-stretch region at  $\Delta_{\text{IFD}} \sim 65\text{ cm}^{-1}$  for different lipids as indicated using the 100 fs laser system (top) and the 5 fs system (center, bottom). The bottom panels show  $\hat{I}_{\text{DCARS}}(x, y)$  images through the center of LDs at  $\nu_{\text{IFD}1}$ , indicated by corresponding dashed lines (blue  $2860\text{ cm}^{-1}$ , black  $2930\text{ cm}^{-1}$ , red  $2997\text{ cm}^{-1}$ ) on a color scale as shown. Pump power on each pair 16 mW, Stokes power on each pair 8 mW, objective  $20 \times 0.75\text{ NA}$ ,  $10\text{ }\mu\text{s}$  pixel dwell time,  $0.3\text{ }\mu\text{m}$  pixel size.

double bonds,  $\hat{I}_{\text{DCARS}}$  at around  $1660\text{ cm}^{-1}$  for GTL even when scaled to the  $1450\text{ cm}^{-1}$  resonance for relative comparison [8] remains comparable to that of GTO. This is attributed to the larger linewidth of the C=C resonance for GTL compared to GTO (see Figure 1) considering that at resonance  $\hat{I}_{\text{DCARS}}$  is scaling as  $I_R/\Gamma$ .

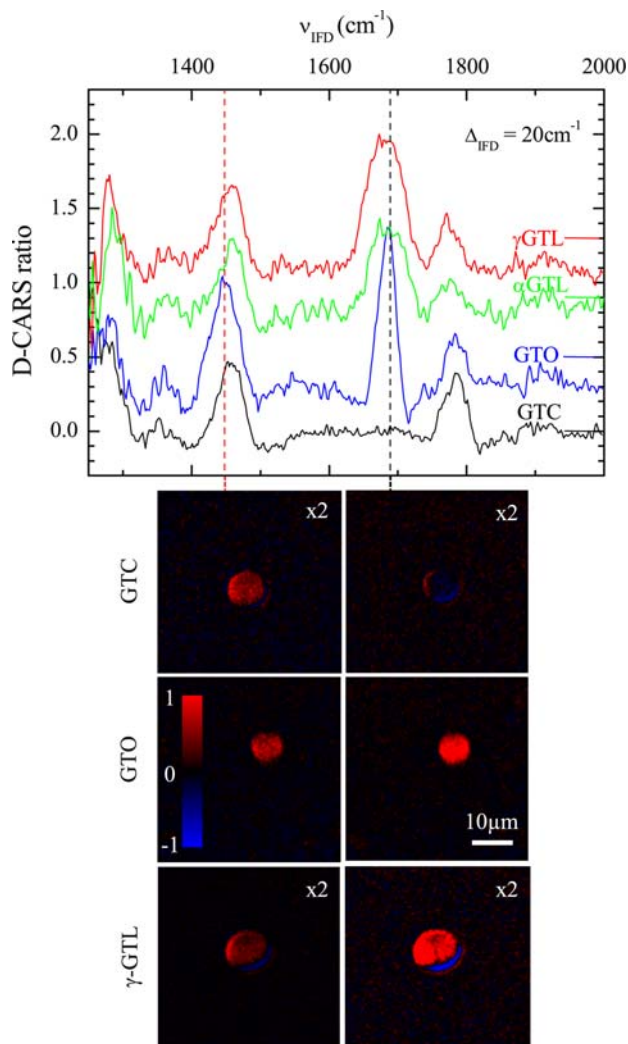


**Figure 6** Measured  $\hat{I}_{\text{DCARS}}$  in the fingerprint region with  $\Delta_{\text{IFD}} = 20 \text{ cm}^{-1}$  for different lipids using the 5 fs system. Curves are vertically displaced for clarity, as indicated by offset lines. The bottom panels show  $\hat{I}_{\text{DCARS}}(x, y)$  images of LDs on a color scale at the two  $\nu_{\text{IFD}1}$  indicated by corresponding dashed lines (red  $1448 \text{ cm}^{-1}$ , black  $1689 \text{ cm}^{-1}$ ).  $\hat{I}_{\text{DCARS}}$  has been multiplied by two in the images for GTC and  $\gamma$ -GTL as indicated, in order to have comparable values at  $1448 \text{ cm}^{-1}$ . Pump power on each pair 16 mW, Stokes power on each pair 8 mW, objective  $20 \times 0.75 \text{ NA}$ ,  $10 \mu\text{s}$  pixel dwell time,  $0.3 \mu\text{m}$  pixel size.

## 4. Conclusions

In summary, we have demonstrated that differential-CARS microscopy using femtosecond pulses spectrally focussed by glass dispersion is able to distinguish poly-unsaturated glyceryl trilinolenate from the more ordered mono-unsaturated glyceryl trioleate and saturated glyceryl tricaprlylate and glyceryl

tristearate without the need of slow CARS multiplex acquisition and analysis. Spectral signatures of disorder which appear in the CH-stretch band of the Raman spectrum at around  $2930 \text{ cm}^{-1}$  correlate well with D-CARS measured as CARS intensity difference between the bands at around  $2930 \text{ cm}^{-1}$  and  $2850 \text{ cm}^{-1}$ . In particular poly-unsaturated glyceryl trilinolenate exhibit a “flat-hat” CARS spectrum with equally intense bands and hence zero D-CARS, while all other lipids exhibit a positive D-CARS. As a proof-of-principle, D-CARS images were acquired on micron-sized lipid droplets at specific wavenumbers to directly distinguish glyceryl trilinolenate from the other lipids based solely on the D-CARS contrast. Similarly, spectral signatures of the degree of poly-unsaturation which appear in the fingerprint region of the Raman spectrum correlate with D-CARS spectra and images and enabled to distinguish the saturated glyceryl tricaprlylate from the unsaturated lipids. Hence by overcoming the slow image acquisition of multiplex CARS and yet demonstrating sufficient chemical specificity to distinguish different lipid types, D-CARS has the potential to enable investigation of lipid composition of cytosolic lipid droplets, label-free, in living cells. We are presently evaluating this potential by imaging stem-cell derived human adipocytes fed with saturated and unsaturated fatty acids to determine differences in lipid chemical contrast with D-CARS. The outcome of this study will be published in a future work.

**Acknowledgements** This work was funded by the UK BBSRC Research Council (grant n. BB/H006575/1). CDN acknowledges financial support by the President’s Research Scholarship programme of Cardiff University, FM acknowledges financial support from the UK EPSRC Research Council (grant n. EP/H45848/1). PB acknowledges the UK EPSRC Research Council for her Leadership fellowship award (grant n. EP/I005072/1). The authors acknowledge the European Union COST action MP0603 “Chemical imaging by means of CARS microscopy (microCARS)” for supporting a short-term mission of IP to the University of Twente to perform some of the Raman spectroscopy shown in this work. The authors also acknowledge scientific discussions and support in LD sample preparation by Peter Watson.

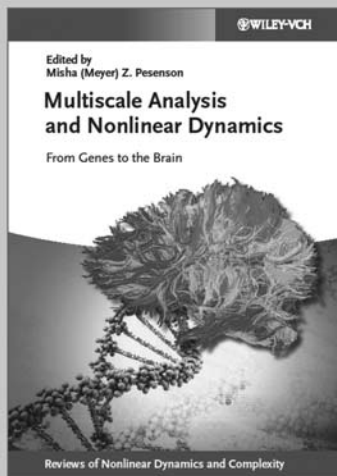
**Author biographies** Please see Supporting Information online.

## References

- [1] M. Digel, R. Eehalt, and J. Füllekrug, *FEBS Letters* **584**, 2168–2175 (2010).
- [2] R. V. Farese and T. C. Walther, *Cell* **139**, 855 (2009).
- [3] L. L. Listenberger and D. A. Brown, *Curr. Protoc. Cell Biol.* **24.2**, 24.2.1 (2007).

- [4] J. Cheng, A. Fujita, Y. Ohsaki, M. Suzuki, Y. Shinohara, and T. Fujimoto, *Histochem. Cell Biol.* **132**, 281 (2009).
- [5] M. Muller and A. Zumbusch, *Chem. Phys. Chem.* **8**, 2156 (2007).
- [6] T. T. Le, S. Yue, and J.-X. Cheng, *J. Lipid Res.* **51**, 3091 (2010).
- [7] J. P. Pezacki, J. A. Blake, D. C. Danielson, D. C. Kennedy, R. K. Lyn, and R. Singaravelu, *Nat. Chem. Biol.* **7**, 137 (2011).
- [8] H. A. Rinia, K. N. J. Burger, M. Bonn, and M. Müller, *Biophys. J.* **95**, 4908 (2008).
- [9] E. M. Vartiainen, H. A. Rinia, M. Müller, and M. Bonn, *Opt. Express* **14**, 3622 (2006).
- [10] I. Rocha-Mendoza, W. Langbein, P. Watson, and P. Borri, *Opt. Lett.* **34**, 2258 (2009).
- [11] W. Langbein, I. Rocha-Mendoza, and P. Borri, *Appl. Phys. Lett.* **95**, 081109 (2009).
- [12] V. V. Pully, A. Lenferink, and C. Otto, *J. Raman Spectrosc.* **41**, 599–608 (2010).
- [13] I. Rocha-Mendoza, W. Langbein, and P. Borri, *Appl. Phys. Lett.* **93**, 201103 (2008).
- [14] I. Pope, W. Langbein, P. Watson, and P. Borri, unpublished.
- [15] P. V. Joke De Gelder, Kris De Gussem, and L. Moens, *J. Raman Spectrosc.* **38**, 1133 (2007).
- [16] S. P. Verma and D. F. Wallach, *Biochim. Biophys. Acta* **486**, 217 (1977).
- [17] R. N. Jones and R. A. Ripley, *Can. J. Chem.* **42**, 305 (1964).
- [18] J. Sebek, L. Pele, E. O. Potma, and R. Benny Gerber, *Phys. Chem. Chem. Phys.* **13**, 12724 (2011).
- [19] W. Langbein, I. Rocha-Mendoza, and P. Borri, *J. Raman Spectrosc.* **40**, 800 (2009).

+++ NEW +++



2013. 328 Pages, Hardcover  
174 Fig. (24 Colored Fig.)  
ISBN 978-3-527-41198-6

Misha (Meyer) Z. Pesenson (ed.)

## Multiscale Analysis and Nonlinear Dynamics: From Genes to the Brain

*Reviews of Nonlinear Dynamics and Complexity (Volume 8)*

Modeling multiscale phenomena in systems biology and neuroscience is a very interdisciplinary task, so the editor of the book invited experts in bio-engineering, chemistry, cardiology, neuroscience, computer science, and applied mathematics, to provide their perspectives. Multiscale analysis is the major integrating theme of the book, as indicated by its title. The subtitle does not call for bridging the scales all the way from genes to behavior, but rather stresses the unifying perspective provided by the concepts referred to in the title. Each

chapter provides a window into the current state of the art in the areas of research discussed. The book is thus intended for advanced researchers interested in recent developments in these fields. It is believed that the interdisciplinary perspective adopted here will be beneficial for all the above-mentioned fields. The roads between different sciences, "while often the quickest shortcut to another part of our own science, are not visible from the viewpoint of one science alone."

Register now for the free  
**WILEY-VCH Newsletter!**  
[www.wiley-vch.de/home/pas](http://www.wiley-vch.de/home/pas)

WILEY-VCH • P.O. Box 10 11 61 • 69451 Weinheim, Germany  
Fax: +49 (0) 62 01 - 60 61 84  
e-mail: [service@wiley-vch.de](mailto:service@wiley-vch.de) • <http://www.wiley-vch.de>

**WILEY-VCH**